

High-Frequency Nanofluidics: An Experimental Study Using Nanomechanical Resonators

D. M. Karabacak, V. Yakhot, and K. L. Ekinci*

Department of Aerospace and Mechanical Engineering, Boston University, Boston, Massachusetts 02215, USA
(Received 8 March 2007; published 22 June 2007)

Here we apply nanomechanical resonators to the study of oscillatory fluid dynamics. A high-resonance-frequency nanomechanical resonator generates a rapidly oscillating flow in a surrounding gaseous environment; the nature of the flow is studied through the flow-resonator interaction. Over the broad frequency and pressure range explored, we observe signs of a transition from Newtonian to non-Newtonian flow at $\omega\tau \approx 1$, where τ is a properly defined fluid relaxation time. The obtained experimental data appear to be in close quantitative agreement with a theory that predicts a purely elastic fluid response as $\omega\tau \rightarrow \infty$.

DOI: 10.1103/PhysRevLett.98.254505

PACS numbers: 47.61.Fg, 47.85.Np, 85.85.+j

The Navier-Stokes equations based upon the Newtonian approximation have been remarkably successful over the centuries in formulating solutions for relevant flow problems both in bulk and near solid walls [1]. The Newtonian approximation breaks down, however, when the particulate nature of the fluid becomes significant to the flow. The Knudsen number $\text{Kn} = \lambda/L$ is one parameter which is commonly used to settle whether the Newtonian approximation can be applied to a medium or not. Here one compares the mean free path λ in the medium to an *ill-defined* characteristic length L . A second defining parameter, especially for oscillatory flow, is the Weissenberg number $\text{Wi} = \tau/T$, which compares the characteristic time scale T of the flow with the relaxation time τ in the medium. As $\tau/T = \omega\tau$ is varied—for instance, by varying the flow frequency ω or the relaxation time τ —the nature of the flow changes drastically.

Recent developments in nanometer-scale engineering have created a vibrant subfield of fluid dynamics called nanofluidics [2]. Most nanofluidics work is concerned with flow in nanoscale channels and remains strictly in the Newtonian regime. In contrast, emerging nanometer-scale mechanical resonators [3,4], with frequencies already extended into the microwaves [5,6], offer an uncharted parameter space for studying nanofluidics. For a high-frequency nanomechanical resonator with resonance frequency $\omega/2\pi$, one can tune $\omega\tau$ over a wide range—in fact, possibly reaching the limits of the Newtonian approximation in a given liquid or gas. This not only allows experimental probing of a flow regime that was inaccessible by past experiments [7,8] but also presents the unique prospect of designing nanodevices for key technological applications.

To complement the recent theoretical interest in high-frequency nanofluidics [2,9–11], we experimentally studied the interaction of high-frequency nanomechanical resonators with a gaseous environment. The gaseous environment presents an ideal fluid for these studies, where one can effectively tune τ by changing the pressure p . On the other hand, varying the resonator dimensions changes the

mechanical resonance frequency $\omega/2\pi$. When combined, the two experimental parameters allow $\omega\tau$ to be varied over several orders of magnitude effectively.

In order to cover a broad frequency range, we fabricated silicon doubly clamped beam resonators with varying dimensions $w \times h \times l$ displayed in Table I using standard techniques [12]. To further extend the frequency range, we employed fundamental and first harmonic modes of two commercial silicon atomic force microscope (AFM) cantilevers (Table I). For the measurements, we used a pressure-controlled optical characterization chamber connected to a high purity N_2 source. We actuated the out-of-plane modes of the resonators electrostatically and measured the displacements optically [12]. All measurements were performed under linear drive; moreover, the results remained independent of the rms displacement amplitudes of ~ 0.1 nm as confirmed by Michelson interferometry. Figure 1 depicts the typical resonant response of a nanomechanical resonator as the background N_2 pressure in the chamber is increased. The frequency shift is due to the

TABLE I. Device parameters, transition pressure $p(\text{Wi} = 1)$, and the approximate lower pressure limit p_{\min} for accurate measurements for the devices used in the study. 1st harmonic mode was also employed for some AFM cantilevers.

$w \times h \times l$ (μm)	$\omega_0/2\pi$ (MHz)	Q_0	$p(\text{Wi} = 1)$ (Torr)	p_{\min} (Torr)
$53 \times 2 \times 460$ (1st harmonic)	0.078	8321	1.0	0.05
$36 \times 3.6 \times 125$ (fundamental)	0.31	8861	3.0	0.05
$36 \times 3.6 \times 125$ (1st harmonic)	1.97	3522	17.5	0.06
$0.50 \times 0.28 \times 17.1$	10.4	1840	110	1.9
$0.50 \times 0.28 \times 11.2$	18.1	1530	200	2.9
$0.93 \times 0.22 \times 9.9$	22.8	1335	176	0.8
$0.76 \times 0.22 \times 9.9$	22.9	1200	216	1.2
$0.23 \times 0.20 \times 9.6$	24.2	415	280	2.77
$0.50 \times 0.28 \times 9.1$	27.1	909	290	2.6
$0.32 \times 0.20 \times 7.7$	33.2	780	320	15.8
$0.50 \times 0.28 \times 5.9$	45.7	1066	310	2.3
$0.25 \times 0.20 \times 5.6$	53.2	571	400	1.2
$0.73 \times 0.23 \times 5.6$	58.6	525	490	19.0
$0.24 \times 0.20 \times 3.6$	102.5	495	...	11.9

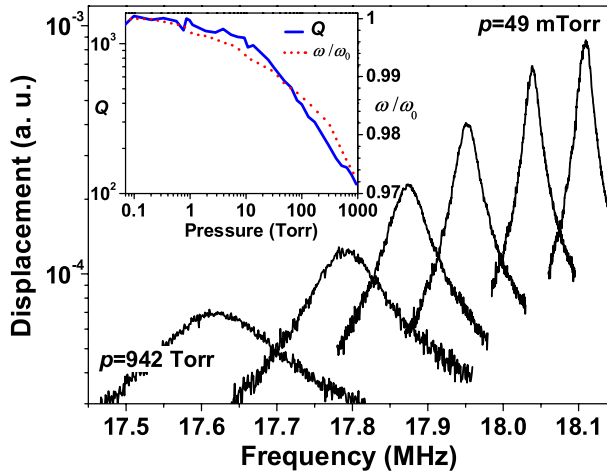


FIG. 1 (color online). Resonance of a silicon doubly clamped beam of width $w = 500$ nm, thickness $h = 280$ nm, and length $l = 11.2$ μm at various N_2 pressures in the chamber: $p = 0.049$, 5.4, 32, 100, 302, and 942 Torr. The inset shows the extracted quality factor Q and normalized resonance frequency ω/ω_0 of the same device as a function of pressure. Here $Q_0 \approx 1530$.

mass loading from the boundary layer [13], while the broadening results from the energy dissipation in the fluid. The analysis can be simplified by using a one-dimensional damped harmonic oscillator approximation [14] $\ddot{x} + \gamma\dot{x} + \omega^2x = f/m$, where f/m represents the force per unit effective mass of the resonator. The quality factor Q , which is a comparison of the stored energy to the dissipated energy per cycle, is related to γ as $\gamma \approx \omega/Q$. Here we extracted both the resonance frequency $\omega/2\pi$ and Q using nonlinear least squares fits to the Lorentzian response of the resonator. In addition, for low Q (high pressure), we verified the Lorentzian fit results through fits to the real and imaginary components of the complex transmission [15]. Typical changes in ω and Q of a nanomechanical resonator during a pressure sweep are shown in the inset in Fig. 1. Both ω and Q approach their respective *intrinsic* values, ω_0 and Q_0 , at low pressure.

Before presenting further results, we must clarify the nature of the fluidic energy dissipation. The motion of the fluid with respect to the solid boundary creates a complex, position-dependent shear stress on the resonator surface. The inertial and dissipative components of the net shear force are proportional to the displacement and the velocity, respectively. For a single device, as the pressure is changed, the fluidic dissipation can be quantified by either the fluidic quality factor Q_f given by $Q_f^{-1} = Q^{-1} - Q_0^{-1}$ or the fluidic dissipation $\gamma_f = \omega/Q_f$. To compare different devices with varying sizes and geometries, one needs to further realize that the fluidic dissipation is proportional to the effective surface area S_{eff} , while the stored energy in the resonator is proportional to the effective mass m [16]. With this naive assumption, we define a normalized fluidic dissipation $\gamma_n = \gamma_f m/S_{\text{eff}}$. The lower pressure limit p_{min} for accurate Q_f measurement is set by Q_0 : As one approaches p_{min} , the intrinsic losses in the resonator dominate the measurement. The upper limit is 1000 Torr. Table I displays p_{min} for each device along with Q_0 .

The normalized fluidic dissipations γ_n observed in three different resonators are presented in Figs. 2(a)–2(c) as a function of gas pressure. A change in the slope is noticeable for the data in Figs. 2(a) and 2(b) at approximate pressures of 1 and 300 Torr, respectively. The turn points marked in the plots correspond to $\omega\tau \approx 1$ and are discussed in detail below. For the highest frequency beam at 102.5 MHz shown in Fig. 2(c), the turn point falls outside the available pressure range, i.e., 1000 Torr. The molecular flow model [10], which takes into account specular collisions, fits our data only at the ideal gas limit at low pressure. Note that a multiplicative constant of 0.9 was used in all three to improve the fits. Viscous effects [17,18] and squeeze-film effects [19,20], commonly observed in microelectromechanical systems, did not introduce significant damping for the small high-frequency devices up to atmospheric pressure.

The solid lines in Fig. 2 are fits to a theory by Yakhot and Colosqui [9] developed from the Boltzmann equation in

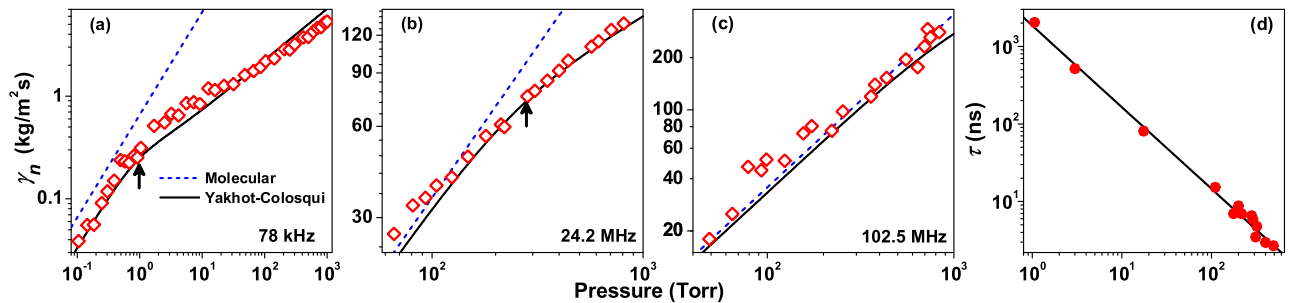


FIG. 2 (color online). Normalized fluidic dissipation γ_n as a function of pressure for (a) a cantilever with dimensions ($w \times h \times l$) $53 \times 2 \times 460$ μm and nanomechanical doubly clamped beams with dimensions of (b) $230 \text{ nm} \times 200 \text{ nm} \times 9.6$ μm and (c) $240 \text{ nm} \times 200 \text{ nm} \times 3.6$ μm . Resonance frequencies are as indicated, and the approximate turning points are marked with arrows. The lines are fits to the molecular collision model [10] and Eq. (1) using $\tau \approx 1850/p$ [9]. The molecular collision and the Yakhot-Colosqui predictions were multiplied by 0.9 and 2.8, respectively, for *all* resonators. (d) Relaxation time τ as a function of pressure. The points were extracted from fluidic dissipation data sets, such as those shown in (a) and (b), of 13 resonators. The solid line is a least-mean-squares fit and indicates that $\tau \approx 1850/p$.

the relaxation time approximation. After geometric normalization and imposing the no-slip boundary condition, this theory culminates in the expression

$$\gamma_n \approx \frac{1}{(1 + \omega^2 \tau^2)^{3/4}} \sqrt{\frac{\omega \mu \rho_f}{2}} \left[(1 + \omega \tau) \cos\left(\frac{\tan^{-1} \omega \tau}{2}\right) - (1 - \omega \tau) \sin\left(\frac{\tan^{-1} \omega \tau}{2}\right) \right]. \quad (1)$$

In Eq. (1), γ_n is expressed in terms of the viscosity μ , the density ρ_f , the effective relaxation time τ of the fluid, and the frequency ω of the resonator. The only unavailable parameter is the relaxation time τ . In order to obtain the fits, we assumed that τ satisfied the empirical form $\tau \propto 1/p$ [8,21]. The key prediction of the Yakhot-Colosqui [9] theory is that the turn point in γ_n occurs when $\tau \approx 1/\omega$. Thus, our experiments provided a direct and unique way to extract τ as a function of pressure p : Figure 2(d) displays the experimentally extracted τ from the transition points of multiple resonators as a function of pressure. Through linear fitting, one can obtain the expression $\tau \approx 1850/p$ (nanoseconds when p is Torr). The end result of this exercise is the self-consistent fits in Figs. 2(a)–2(c). To improve the fits, the results emerging from Eq. (1) with the appropriate material properties and τ were multiplied by 2.8. In general, *all* our data sets could be fit adequately using Eq. (1) after multiplying by 2.8 ± 0.7 .

The fluidic dissipation in individual resonators shown in Fig. 2 suggests that there, indeed, is a transition at $\omega \tau \approx 1$, obtained by tuning τ . Further support for this transition comes from extended measurements in the frequency parameter space. Figure 3(a) shows γ_n from different resonators spanning a huge frequency range. Here γ_n is plotted against the resonator frequency ω_0 at four different pressures [16], i.e., four different τ . This comparison between different devices with different sizes is possible only after normalization of the dissipation by S_{eff}/m [22]. The solid lines in Fig. 3(a) are fits to Eq. (1) using $\tau \approx 1850/p$. The points marked by arrows correspond to $\omega \tau \approx 1$. Again, we have multiplied all of the fits by 2.8 as in Fig. 2. This multiplicative constant probably arises from adapting the theoretical expressions [9] for an infinite plate oscillating *in plane* to the finite and rectangular resonators oscillating *out of plane*. Our surface-to-volume normalization does not give the absolute dissipation, while it appears to be useful for comparing different devices. The elucidation of finite size effects in complex geometries is the subject of our ongoing computational research. Figure 3(b) shows all of the data, $\gamma_n / \sqrt{\omega \mu \rho_f}$, from all devices collapsed onto a single curve, plotted against over four decades of the dimensionless parameter $\text{Wi} = \omega \tau$. Each symbol type in Fig. 3(b) corresponds to a separate resonator; Wi is obtained by multiplying the resonator frequency by the corresponding τ from $\tau \approx 1850/p$. The solid curve is obtained from Eq. (1).

Also apparent in Fig. 1 is a small decrease in the resonance frequency as the pressure is increased. The

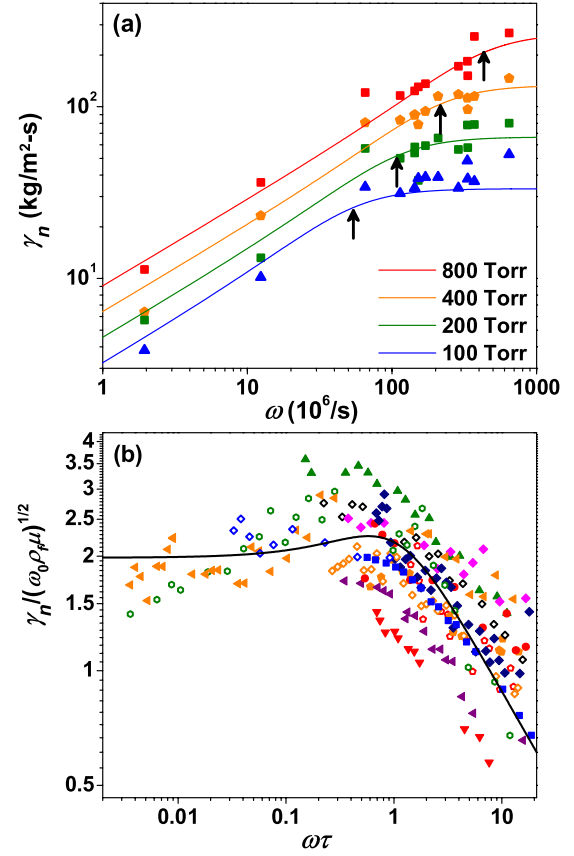


FIG. 3 (color online). (a) Normalized fluidic dissipation γ_n as a function of the resonator frequency ω_0 for several resonators at four different pressures. From top to bottom, $\tau \approx 2.3, 4.6, 9.2,$ and 18.5 ns. The lines are fits calculated using Eq. (1). $\text{Wi} \approx 1$ points are marked with an arrow for each pressure. (b) The scaling of $\gamma_n / \sqrt{\omega \mu \rho_f}$ for all resonators with $\omega \tau$. Each symbol corresponds to an individual resonator. *All* of the predictions were multiplied by the same fitting factor of 2.8 (also see Fig. 2).

observed decrease is primarily due to the mass of the fluid m_f that is being displaced in phase with the resonator: $\Delta \omega / \omega_0 \approx m_f / 2m$ [4]. Both the geometry and the frequency of the moving surface are expected to play a role in determining m_f and, thus, $\Delta \omega$. In an effort to rule out the geometry effects, we studied the frequency shift in four beams of *identical* widths ($w = 500$ nm) and thicknesses ($h = 280$ nm) but varying lengths and resonance frequencies as a function of pressure (Fig. 4). Here the plotted $\Delta \omega / \omega_0$ corresponds to the approximate *fluid mass per unit beam length*. The arrows mark $\text{Wi} \approx 1$ for each beam, and the dashed lines represent best line fits corresponding to $\Delta \omega \propto p^{1/3}$. The molecular flow model [10], which is appropriate at low pressure, does not predict any mass loading and frequency shift. At high pressure, the Stokes expression for an oscillating plate [1] can be used to obtain an approximation for the boundary layer thickness $\delta = \sqrt{2\mu / \rho_f \omega}$. This, however, results in a pressure-independent $\Delta \omega$, given that typically $\delta \sim 1\text{--}5$ μm , and, consequently, $m_f / m \approx \rho_f \delta^2 / \rho_s w h$. The Yakhot-Colosqui

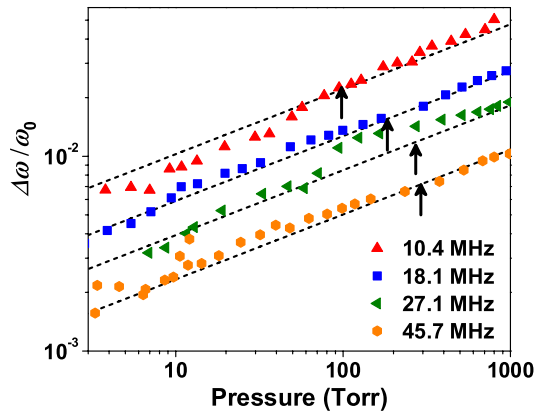


FIG. 4 (color online). Normalized frequency $\Delta\omega/\omega_0$ for beams of *identical* widths $w = 500$ nm and thicknesses $h = 280$ nm but varying lengths and resonance frequencies. The pressure for $Wi \approx 1$ is marked with an arrow. Dashed lines are least-mean-squares fits to $\Delta\omega \propto p^{1/3}$.

theory [9] underestimates the magnitude of the observed frequency shift. We expect to understand the nature of the boundary layer in the near future by studying the scaling of experimental frequency shifts in a wide range of geometries and frequencies and through supporting computational analyses.

The transition observed in our experiments can be interpreted in the most general terms as follows. The simple linear relation between stress and rate of strain in a Newtonian fluid breaks down at high frequencies. The Boltzmannian theory developed by Yakhot and Colosqui suggests that this result is *independent* of the nature of the fluid. This transition at $Wi = \omega\tau \approx 1$ was described [9] as a “viscoelastic to elastic” transition owing to the fact that the waves generated in the fluid by the resonator motion do *not* decay as $\omega \rightarrow \infty$. There also appears to be some universality with respect to device geometry: In both cantilevers and doubly clamped beams, the same naive geometric normalization resulted in a consistent analysis.

There is a relentless effort to develop nanomechanical resonators operating in gaseous [23] and liquid environments [24]. Our results should impact the design of next-generation nanomechanical resonators. Figure 3 suggests that fluidic dissipation saturates at high frequencies. Take, for instance, two doubly clamped beam resonators with identical widths and thicknesses but different lengths, i.e., identical $S_{\text{eff}}/m \approx \frac{1}{w} + \frac{1}{h}$ but different frequencies such that $\omega_1 < \omega_2$. If $\omega_1 < \omega_2 < 1/\tau$, the ratio of the quality factors of the two resonators in fluid becomes $Q_{2f}/Q_{1f} \sim \sqrt{\omega_2/\omega_1}$. On the other hand, if $\omega_1 < 1/\tau < \omega_2$, then $Q_{2f}/Q_{1f} \sim \omega_2\sqrt{\tau/\omega_1}$. Finally, for $1/\tau < \omega_1 < \omega_2$, $Q_{2f}/Q_{1f} \sim \omega_2/\omega_1$. Thus, a shorter, higher-frequency resonator will always be more resilient in a given fluid, but the degree of resilience depends upon the fluid τ . Yet, for two devices with identical frequencies, the smaller one with the larger S_{eff}/m will have the lower Q_f . For the case

where both S_{eff}/m and the device frequency increase, the nature of the scaling determines the end result. Finally, the surface roughness, especially for very small devices, is expected to have an important role in the nanofluidics of nanomechanical resonators [25].

We thank M. Paul, A. Vandelay, C. Colosqui, and R. Bhiladvala for helpful conversations. We acknowledge generous support from NSF through Grants No. CMS-324416 and No. BES-216274.

*To whom all correspondence should be addressed.
ekinci@bu.edu

- [1] L. D. Landau and E. M. Lifshitz, *Fluid Mechanics* (Butterworth-Heinemann, Oxford, 1987), 2nd ed.
- [2] G. Karniadakis, A. Beskok, and N. Aluru, *Microflows and Nanoflows* (Springer, New York, 2005), 1st ed.
- [3] M. L. Roukes, *Sci. Am.* **285**, No. 9, 48 (2001); H. G. Craighead, *Science* **290**, 1532 (2000).
- [4] K. L. Ekinci and M. L. Roukes, *Rev. Sci. Instrum.* **76**, 061101 (2005).
- [5] X. M. H. Huang *et al.*, *Nature (London)* **421**, 496 (2003).
- [6] H. B. Peng *et al.*, *Phys. Rev. Lett.* **97**, 087203 (2006).
- [7] J. T. Tough, W. D. McCormick, and J. G. Dash, *Phys. Rev.* **132**, 2373 (1963); L. Bruschi and M. Santini, *Rev. Sci. Instrum.* **46**, 1560 (1975); P. I. Oden *et al.*, *Appl. Phys. Lett.* **68**, 3814 (1996); Y. Xu *et al.*, *Appl. Phys. Lett.* **88**, 143513 (2006).
- [8] M. Rodahl *et al.*, *Rev. Sci. Instrum.* **66**, 3924 (1995).
- [9] V. Yakhot and C. Colosqui, arXiv:nlin/0609061v4; *J. Fluid Mech.* (to be published).
- [10] R. B. Bhiladvala and Z. J. Wang, *Phys. Rev. E* **69**, 036307 (2004).
- [11] M. R. Paul and M. C. Cross, *Phys. Rev. Lett.* **92**, 235501 (2004).
- [12] T. Kouh *et al.*, *Appl. Phys. Lett.* **86**, 013106 (2005).
- [13] The virtual mass effect due to the potential flow around the structure was determined to be negligible.
- [14] A. Cleland, *Foundations of Nanomechanics* (Springer, New York, 2003), 1st ed.
- [15] P. J. Petersan and S. M. Anlage, *J. Appl. Phys.* **84**, 3392 (1998).
- [16] The typical mass loading in these experiments is small. Thus, for all practical purposes, $\omega \approx \omega_0$.
- [17] J. E. Sader, *J. Appl. Phys.* **84**, 64 (1998).
- [18] F. R. Blom *et al.*, *J. Vac. Sci. Technol. B* **10**, 19 (1992).
- [19] J. L. T. Veijola, H. Kuisma, and T. Ryhanen, *Sens. Actuators A, Phys.* **48**, 239 (1995).
- [20] J. J. Blech, *J. Lubr. Technol.* **105**, 615 (1983).
- [21] E. T. Watts, J. Krim, and A. Widom, *Phys. Rev. B* **41**, 3466 (1990).
- [22] $S_{\text{eff}} \approx 2l(w+h)$; $m \approx Clwh\rho$; the value of C depends upon the structure geometry and the mode shape. A distributed force approximation for calculating C was appropriate for our experimental conditions.
- [23] M. Li, H. X. Tang, and M. L. Roukes, *Nature Nanotechnology* **2**, 114 (2007).
- [24] S. S. Verbridge *et al.*, *Nano Lett.* **6**, 2109 (2006).
- [25] G. Palasantzas, *Appl. Phys. Lett.* **90**, 041914 (2007).